RSC Advances

PAPER

View Article Online
View Journal | View Issue

Cite this: *RSC Adv.*, 2024, **14**, 21971

Nucleating and reinforcing effects of nanobiochar on poly(3-hydroxybutyrate-*co*-3-hydroxhexanoate) bionanocomposites

Lawrence Yee Foong Ng,[a] Hidayah Ariffin,[*ab] Tengku Arisyah Tengku Yasim-Anuar,[bc] Megumi Sakata,[†d] Tomoya Kawarada,[d] Osamu Yoshimura,[d] Takayuki Tsukegi,[d] Nik Mohd Afizan Nik Abd Rahman[ae] and Mohd Ali Hassan[b]

Received 21st December 2023
Accepted 25th April 2024

DOI: 10.1039/d3ra08721b

rsc.li/rsc-advances

This study promotes the use of nanobiochar (NBC) as an environmentally friendly substitute to conventional fillers to improve various properties of biopolymers such as their mechanical strength, thermal stability and crystallization properties. TGA analysis showed a slight increase in onset thermal degradation temperature of the composites by up to 5 °C with the addition of 4 wt% NBC. Non-isothermal DSC analysis determined that the addition of NBC into PHBHHx increases the crystallization temperature and degree of crystallinity of PHBHHx while isothermal DSC analysis demonstrated higher crystallization rate in PHBHHx/NBC composited by up to 54%. PHBHHx incorporated with NBC also exhibited superior tensile strength and modulus *versus* neat PHBHHx. Increase in mechanical strength was further proven *via* DMA where PHBHHx/NBC composites maintained higher storage modulus at higher temperatures when compared to neat PHBHHx. PHBHHx/NBC also exhibited no cytotoxicity effect against HaCat cells. This study demonstrates the ability of biochar to act as both nucleating agents and reinforcing agents in biodegradable polymers such as PHBHHx, which could be suitable for packaging application.

Introduction

One of the major factors contributing to the decline of the environmental state of the planet is the use and irresponsible disposal of conventional single-use plastics. The rampant use of single-use plastics is due to the exceptional properties of these polymers in terms of their mechanical and thermal properties in addition to their ease of manufacturing. These advantages lead to a myriad of potential applications which include, but are not limited to disposable cutlery, food packaging and clothing such as disposable raincoats. However, traditional plastics that are used in most of the single-use plastic products are non-biodegradable and take up to 1000 years to decompose in landfills and this has led to the harmful build-up of these materials resulting in increasingly severe damage to the ecosystem and the biosphere.[1]

Rising interests in sustainable, renewable materials as alternatives to lessen the impacts of non-biodegradable plastic waste have brought the attention of researchers and the industry towards biopolymers. Biopolymers like poly(3-hydroxybutyrate-*co*-3-hydroxhexanoate) (PHBHHx), a type of medium-chain length polyhydroxyalkanoate (PHA), have several advantages over their fossil-fuel based counterparts, particularly in regard to the single-use plastic packaging industry due to their biodegradability.[2] PHAs in general have biodegradability rates comparable to cellulose and are some of the few types of biopolymers that can biodegrade in river and sea water, with PHBHHx being capable of biodegradation rates of up to 90% mass loss within 90 days.[3,4] PHBHHx, depending on its HHx composition, also has comparable mechanical properties to conventional polymers making it durable enough to withstand the mechanical stress typically applied to packaging materials.[5–7] However, PHBHHx has been known to have lower thermal stability with PHBHHx having onset degradation temperatures ($T_{d\ onset}$) around 290 °C for PHBHHx (10.5 mol% HHx) when compared to polypropylene (PP) and low-density polyethylene (LDPE) with $T_{d\ onset}$ of 384 °C and 392 °C.[8–10] This may lead to stricter moulding/shaping temperature parameters and limiting their applications. When it comes to packaging that need to withstand higher temperatures in applications such as reheatable food packaging or airline

[a]*Laboratory of Biopolymers and Derivatives, Institute of Tropical Forestry and Forest Products (INTROP), Universiti Putra Malaysia, 43400 UPM Serdang, Selangor, Malaysia. E-mail: lawrenceyfng@gmail.com; hidayah@upm.edu.my*

[b]*Department of Bioprocess Technology, Faculty of Biotechnology and Biomolecular Sciences, Universiti Putra Malaysia, 43400 UPM Serdang, Selangor, Malaysia*

[c]*Nextgreen Pulp & Paper Sdn. Bhd., Green Technology Park, Paloh Inai, 26600 Pekan, Pahang, Malaysia*

[d]*Department of Applied Chemistry, Faculty of Biotechnology and Chemistry, Kanazawa Institute of Technology, 7-1 Ohgigaoka, Nonoichi, Ishikawa 921-8501, Japan*

[e]*Department of Cell and Molecular Biology, Faculty of Biotechnology and Biomolecular Sciences, Universiti Putra Malaysia, 43400 UPM Serdang, Selangor, Malaysia*

† Megumi Sakata could not be contacted to confirm the final author list prior to acceptance.

catering where internal food temperatures must reach minimum temperatures ranging from 65 °C to 74 °C, the packaging material should ideally be able to maintain their mechanical strength at these higher temperatures.[11] Additionally, the crystallisation rate of PHBHHx has also been shown to be very slow, even at lower 3-HHx contents, making it difficult to process.[12] Therefore, nucleating agents and reinforcing fillers must be incorporated into the polymer to improve its properties to be more competitive with the conventional polymers currently in the market.

Biochar is a biogenic carbonaceous material derived from the thermal decomposition of biomass achieved under oxygen limiting conditions in a process known as pyrolysis.[13] Biochar is typically used in the agricultural and environmental fields due to is large specific surface area which enables them to act as adsorbents for the slow release of fertilisers into soil or to remove harmful pollutants from the environment.[14] However, biochar has also been found to be able to improve the thermal stability of polymers. Multiple studies have shown that the addition of biochar to polypropylene significantly delays the onset of thermal decomposition to a higher temperature.[13,15,16] Other polymers such as polyvinyl alcohol, high density polyethylene and polyethylene teraphtalate also showed increased thermal stability with the addition of biochar.[17–19] Additionally, it was demonstrated that HDPE/biochar composites showed higher storage modulus at elevated temperatures as the biochar content increases.[18]

It has been well documented that when dealing with fillers for polymers, the particle size of the fillers matter. The extremely high surface area of nanoparticles or nano-sized fillers allows for better dispersion and increased interaction between the filler and the polymer matrix.[20,21] Moreover, due to their better dispersion within the polymer matrix, the resulting composite may show superior improvements in the properties of polymers. This has also been previously demonstrated with nanobiochar (NBC) in a study conducted by Richard *et al.* (2017), where the authors found that the impact strength of polyesters improved significantly with the addition of a small amount of NBC of 45 nm in size compared to composites mixed with larger sized biochar particles. Studies have also found that particles of smaller sizes lead to better nucleation capabilities.[23] The nucleation effect of NBC on PHBHHx will also be investigated in this study.

In this study, NBC produced from oil-palm biomass was used as a reinforcing agent in PHBHHx. The study seeks to improve the thermal stability of PHBHHx with the addition of NBC as well as to evaluate its effects on the crystallinity, mechanical and viscoelastic properties on PHBHHx.

Experimental

Materials

Biochar was produced from pyrolysis of OPEFB at temperature of 500 °C for 25 min in a tubular furnace (Dentsply Ceramco, USA) with a nitrogen flow rate of 258 ml min^{-1} 95% ethanol was purchased from Systerm Chemicals, Malaysia. PHBHHx (6% HHx) in powdered form was generously provided by Kaneka Corporation.

Production of nanobiochar (NBC)

The method used to produce nanobiochar is adopted from our previous study.[24] OPEFB biochar was subjected to mechanical grinding using a commercial kitchen blender to produce biochar powder. The biochar powder was then ground into NBC *via* ball milling using a SPEX 8000D high-energy ball mill with two 60 ml hardened steel vials. The grinding media used consisted of stainless-steel balls of varying sizes ranging from 2.5–11 mm in diameter. Each run of ball milling was done with a duration of 60 minutes and a ball to powder mass ratio of 10 : 1.

Demineralisation of NBC

The resulting NBC was then demineralised *via* acid treatment modified from a method described by.[25] 2 M HCl was added into NBC with a 20 : 1 HCl/NBC weight ratio and left in a shaker for 24 hours. The HCl was then removed from the NBC *via* ultracentrifugation at 10,000 rpm. This was followed by addition of 1 M : 1M HCl–HF to the same weight ratio and left in a shaker for an additional 24 hours. Retrieval of the demineralised NBC was done *via* ultracentrifugation and multiple rinsing steps using deionised water before drying in an oven at 100 °C for 24 hours.

Morphology and mineral content of NBC and dispersion of NBC in polymer matrix

The mineral content of NBC before and after acid treatment were determined using a FEI Nova NanoSEM 230 field emission scanning electron microscope (FESEM) attached with an Oxford X-max energy dispersive X-ray analyser (EDX). Transmission electron microscopy (TEM) was used to visualize the dispersion of NBC within the polymer matrix. TEM images were obtained using a JEOL JEM 2100F Field Emission TEM (JEOL, Tokyo, Japan). A thin layer of composite was sectioned at −80 °C using an ultramicrotome and placed on a copper grid for viewing.

Particle size distribution of NBC

Particle size distribution of NBC was determined *via* dynamic light scattering (DLS) using a Zetasizer NanoS instrument (Malvern Instruments, UK). Sample preparation was done by weighing 1 mg of biochar and NBC and dispersing into 50% ethanol solution. Dispersion of samples were aided by magnetic stirring for 20 min followed by ultrasonication in an ice water bath for an additional 20 min.

Fabrication of PHBHHx/NBC nanocomposites

PHBHHx/NBC nanocomposites were prepared *via* internal melt-blending using a Brabender Plasticoder (Brabender Messtechnik GmbH Co., Duisburg, Germany) internal mixer. Both PHBHHx and NBC were dried in an oven and left in a desiccator prior to melt-blending. The PHBHHx powder was pre-mixed with NBC at different loadings ranging from 1–5 wt%. The resulting mixture was then introduced into the internal mixer at

Table 1 PHBHHx/NBC composites and naming scheme

NBC content, wt%	Designated name
0	Neat PHBHHx
1	N1
2	N2
3	N3
4	N4
5	N5

160 °C and 70 rpm for 10 min. The resulting composite sheets and the designated naming scheme is compiled in Table 1.

Compression moulding was done at 160 °C and 110 kg m^{-2} for 10 min with a preheat time of 10 min to produced composite sheets with a thickness of 1 mm.

Thermogravimetric analysis (TGA)

Thermal stability of neat PHBHHx and composites were assessed using a thermogravimetric analyser (TGA) (TGA 4000, PerkinElmer). Approximately 10 mg of biochar samples were loaded onto a ceramic pan. The samples were held at 50 °C for 1 min before heating up to 400 °C with a heating rate of 10° C min^{-1}. A nitrogen gas flowrate of 20 ml min^{-1} was applied. The TG and derivative thermogravimetry (DTG) curves were obtained from each run.

Differential scanning calorimetry (DSC)

DSC were conducted using the Hitachi Nexta DSC600 This analysis was split into non-isothermal and isothermal DSC analysis.

Non-isothermal DSC. Non-isothermal DSC analysis was conducted by first heating the samples from room temperature to 170 °C with a heating rate of 10 °C min^{-1} and held at that temperature for 3 minutes to remove thermal history. The samples were then cooled at 5 °C min^{-1} to −20 °C before reheating to 170 °C at 10 °C min^{-1} to obtain the second heating thermogram.

Neat PHBHHx and N2 were also cooled at 50 °C min^{-1} to −20 °C in a separate run of non-isothermal DSC analysis to further determine the nucleating effects of NBC. The heating rates for this run was maintained at 10 °C min^{-1}.

Isothermal DSC. Isothermal DSC analysis was conducted by heating the samples from room temperature to 170 °C with a heating rate of 10 °C min^{-1} and held at that temperature for 3 minutes to remove thermal history. The samples were then cooled rapidly at 50 °C min^{-1} to 100 °C. The temperature was then held at 100 °C for 30 min to allows for the isothermal crystallisation of PHBHHx and its composites to occur. The samples were then cooled to 25 °C before heating up to 170 °C at 10 °C min^{-1}.

Tensile properties

Tensile properties were conducted in accordance with ASTM D-638 type V. The compression moulded 1 mm sheets were cut into dumbbell shaped specimens with the measurements specified in the standard. A gauge length (G) of 7.62 mm with a 25.4 mm distance between the grips (D) were used. A minimum of 5 samples were tested with a speed of 1 mm min^{-1} and the average values and standard deviations were calculated.

Dynamic mechanical properties

Dynamic mechanical analysis (DMA) was conducted using the DMA Q800 (TA Instruments) in tensile mode. Samples were compression moulded and cut into specimens with dimensions of 21 × 5 × 0.5 mm. Testing was done with a temperature range from −20 to 110 °C with a heating range of 5 °C min^{-1} and at a constant frequency of 1 Hz.

Morphology observation and *in vitro* cytotoxicity assay on HaCat cells

For cell morphology analysis, human epidermal keratinocytes (HaCat) cells were used and prepared using the same procedures as described by Hussin *et al.* (2018).[26] The HaCat cells were seeded at a density of 2 × 10^4 cells/well in a 96-well plate in Dulbecco Minimum Essential Medium (DMEM) supplemented with 10% fetal bovine serum (FBS) and 1% antibiotics (penicillin, streptomycin, and neomycin), and cultured at 37 °C in a humidified environment with 5% CO_2. The bionanocomposite samples (PHBHHx and PHBHHx/NBC) were prepared by cutting them into small diameter pieces with 5.0 mg and soaking them in 70% ethanol for 1 h. The samples were then sterilised under UV light in laminar airflow for 4 h before been introduced to the wells and incubated under standard conditions for 24 h, 48 h and 72 h. After 24 h, the cells were washed once with PBS and cell viability was observed under an inverted microscope integrated with camera (Nikon, Japan). The same steps were repeated for 48 h and 72 h.

For *in vitro* cytotoxicity analysis, the HaCat cells were sub-cultured upon reaching 80–90% confluency. After 24 h, the

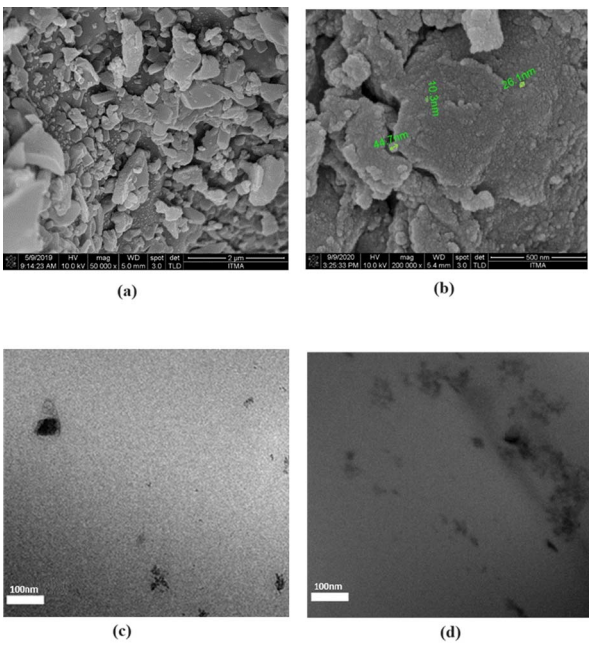

Fig. 1 FESEM images of (a) OPEFB biochar before ball milling (b) OPEFB NBC after ball milling and demineralisation and TEM images of (c) N3 and (d) N5.

culture medium was replaced with fresh medium, and 5.0 mg of each sample (PHBHHx and PHBHHx/NBC) was added into the wells for 24 h, 48 h, and 72 h, respectively. After incubation, the cells were washed once with PBS. Then, 20 μl of MTT solution (5 mg ml^{-1} in PBS) was added into each well and incubated for 4 h in the incubator. Once the purple precipitate was apparent, the media was removed, and 100 μl of DMSO was added to each well. The plate was covered with aluminium foil and incubated for 2 h in the incubator. The cell viability was evaluated using an ELISA microplate reader (Biotech Instruments, USA) with absorbance at 570 nm. The MTT assay was repeated for the 24 h, 48 h and 72 h time points, respectively. The percentage of cell viability was calculated based on the absorbance data, which indicate cell viability using an equation:[27]

$$\text{Cell viability}(\%) = \frac{A_{\text{film}}}{A_{\text{control}}} \times 100\%$$

where A_{film} and A_{control} are absorbance values at 570 nm of the cells with the films and control, in which the cells were cultured in medium without any composite films, respectively. Each experiment was conducted in triplicates.

Results and discussion

Morphology and mineral content of NBC and dispersion of NBC in polymer matrix

The morphology of the biochar before and after ball milling and demineralisation was observed *via* FESEM (Fig. 1). Fig. 1a shows biochar particles after mechanical grinding before ball milling. The biochar particles exist in the form of irregular shapes with large sizes spanning a few micrometres. From Fig. 1b, it can be seen that the large biochar pieces have been broken down into nanoparticles with diameters as small as 10 nm existing in the form of aggregates. Further characterization *via* DLS determined that the average diameter for the NBC produced was approximately 80–90 nm as shown in Fig. 2.

The elemental composition of the NBC particles was determined *via* EDX attached to the FESEM. Previous studies have described that some elements commonly found in biochar, namely Ca and Mg have been known to act as catalysts for the thermal degradation of PHAs.[28] Therefore, demineralisation of the biochar is necessary to remove any unwanted metallic elements that could cause undesired degradation of PHBHHx during melt compounding. This was done by submerging the NBC in HCl followed by a HCl/HF mixture to dissolve the undesired metals and minerals before several rinsing steps with deionized water. The elemental composition of the NBC particles before and after demineralisation was determined *via* EDX. It can be seen from Table 2 that the metal elements (especially Ca and Mg) have been successfully removed from the NBC particles. As a result, the relative carbon content of NBC has also been increased after demineralisation.

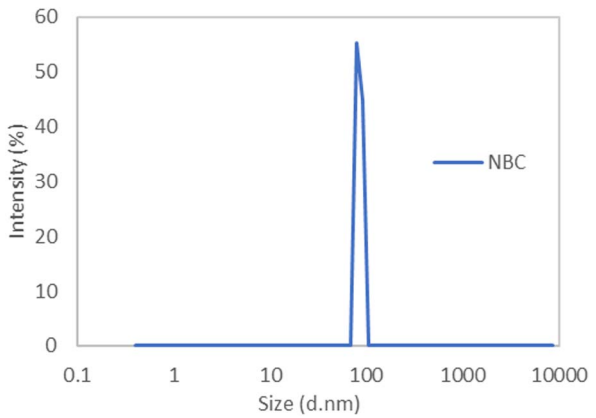

Fig. 2 Particle size distribution of NBC measured *via* DLS.

The elemental composition of the NBC particles was determined *via* EDX attached to the FESEM. Previous studies have described that some elements commonly found in biochar, namely Ca and Mg have been known to act as catalysts for the thermal degradation of PHAs.[28] Therefore, demineralisation of the biochar is necessary to remove any unwanted metallic elements that could cause undesired degradation of PHBHHx during melt compounding.

This was done by submerging the NBC in HCl followed by a HCl/HF mixture to dissolve the undesired metals and minerals before several rinsing steps with deionized water. The elemental composition of the NBC particles before and after demineralisation was determined *via* EDX. It can be seen from Table 2 that the metal elements (especially Ca and Mg) have been successfully removed from the NBC particles. As a result, the relative carbon content of NBC has also been increased after demineralisation.

The dispersion of NBC within the PHBHHx matrix was visualised in Fig. 1c and d *via* TEM. At 3% NBC loading (Fig. 1c), the NBC particles were well disperse in the PHBHHx matrix where individual particles below 100 nm could be clearly seen. However, as the composition of the NBC increased to 5% (Fig. 1d), the NBC particles started to agglomerate due to physical interactions between the nanoparticles.

Thermal stability

TGA analysis was done to compare the thermal stability of NBC composites with those of neat PHBHHx. From Fig. 3a, it can be seen that the addition of NBC into PHBHHx led to a slight increase in the thermal stability of the resulting composites, as

Table 2 Elemental composition of biochar and NBC after demineralisation

	Elemental composition (weight %)	
Elements	Untreated NBC	NBC after demineralisation
C	71.22	77.05
O	16.28	20.03
F	0.82	0.83
Mg	0.35	0
Si	1.32	1.52
Cl	2.38	0.56
K	5.47	0
Ca	0.49	0
Fe	1.67	0

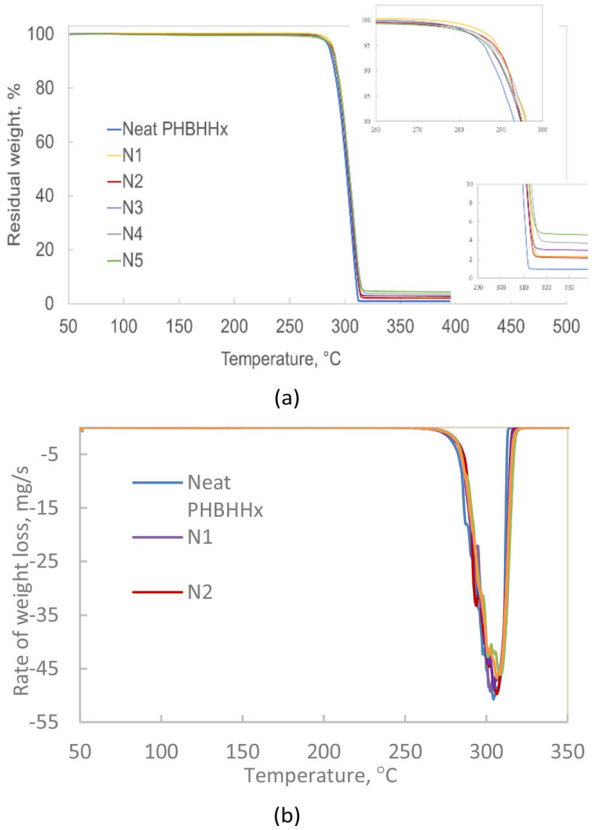

Fig. 3 (a) TGA and (b) DTG thermograms for PHBHHx and NBC composites.

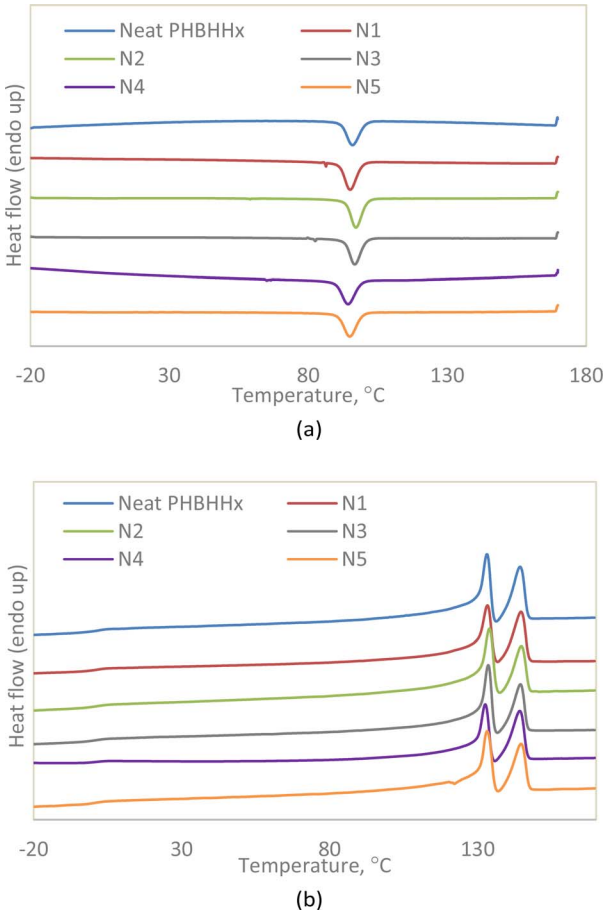

Fig. 4 (a) Non-isothermal cooling curve (5 °C min^{-1}). (b) Second heating curve (10 °C min^{-1}) of PHBHHx and NBC composites.

shown by the onset temperature and residual weight. Single peak degradation shown in the DTG curve indicates that NBC does not significantly impact the thermal degradation behaviour of PHBHHx.

The extrapolated onset of degradation ($T_{d\ onset}$) and thermal degradation temperature at 50% weight loss ($T_{d\ 50\%}$) for the composites also showed no significant increase when compared to that of neat PHBHHx. The negligible increase in the thermal stability may be a result of the low composition of NBC used in the composites. Multiple studies have demonstrated the ability of biochar to consistently improve the thermal stability of a range of polymers.[17,19,29] However, the studies also show that the degree of increase in the thermal stability of the resulting composites is proportional to the amount of biochar used in the composites. In a study by Nan *et al.*, (2015), it was found that the addition of 2 wt% biochar was not sufficient to improve the thermal stability of PVA. The thermal stability of PVA only increased with the addition of more than 6 wt% of biochar. Similarly, Idrees *et al.*, (2018) discovered that thermal stability of PET/biochar composites under inert conditions had minute improvements compared to neat PET. The biochar loading used in their study was 0.5–5 wt%, similar to the biochar loadings used in this study.

Differential scanning calorimetry (DSC)

Non-isothermal DSC. The data for non-isothermal DSC analysis is compiled in Fig. 4a and Table 3 shows the non-isothermal crystallisation profiles of PHBHHx and NBC composites when cooled at 5 °C min^{-1} after their thermal history has been removed *via* the first heating phase. There is a slight shift in the onset of crystallisation ($T_{c\ onset}$) towards a higher temperature when NBC is incorporated into PHBHHx. This is especially evident for N2 with a $T_{c\ onset}$ of 107 °C as compared to the 104 °C of neat PHBHHx. This is indicative of the ability of NBC to act as nucleation sites to trigger spherulite formation, allowing for earlier onset of PHBHHx exothermic crystallisation. As seen in Fig. 4b, PHBHHx has a characteristic melting endotherm with multiple peaks. As explained by Hu *et al.* (2007),[30] the first melting peak is caused by the melting of imperfect crystals followed by the melting of crystals formed during primary crystallisation. While the incorporation of NBC had no significant effect on the melting temperatures (T_{m1}, T_{m2}) of PHBHHx, the melting enthalpy (ΔH_m) slightly increases with the addition of up to 3 wt% of NBC. Consequently, the degree of crystallisation (X_c) slightly increases from 31.3% of neat PHBHHx to 33.3% of N3. The drop in X_c, $T_{c\ onset}$ and T_c with further increase in NBC content beyond N3 can be attributed to the restriction in polymer chain mobility due to excessive NBC and agglomeration which in turn inhibits the formation of spherulites.[31]

To further emphasise on the nucleating effects of NBC, a separate non-isothermal DSC run was conducted on neat

Table 3 Non-isothermal DSC data for PHBHHx and NBC composites with cooling rate of 5 °C min^{-1}

Sample	$T_{c\ onset}$ °C	T_c °C	ΔH_c J g^{-1}	T_{m1} °C	T_{m2} °C	ΔH_m J g^{-1}	X_c %
Neat PHBHHx	104	96	42	133	144	45.7	31.3
N1	105	95	49	133	145	46.0	31.5
N2	107	97	49	134	145	46.5	31.8
N3	106	97	47	134	144	48.6	33.3
N4	104	94	46	133	144	42.8	29.3
N5	105	95	42	133	145	39.3	26.9

PHBHHx and N2 with a cooling rate of 50 °C min^{-1} followed by a second heating step with a heating rate of 10 °C min^{-1} as seen in Fig. 5. As listed in Table 4, the crystallisation enthalpy (ΔH_c) of Neat PHBHHx was lower than that of N2 indicating better crystallisation properties for N2. The ΔH_c of both neat PHBHHx and N2 decreases dramatically as compared to the same samples cooled at 5 °C min^{-1}. This is to be expected as a faster cooling rate would result in less time for the nucleation and crystallisation of the polymer. However, with the increase in cooling rate, the nucleating capabilities of NBC become more obvious. This can be seen in the second heating curves of neat PHBHHx and N2 where the melting peaks for neat PHBHHx is barely visible whereas the characteristic two peak melting endotherm is still visible for N2 albeit less pronounced when compared to the peaks from the same sample cooled at 5 °C min^{-1}. The rapid cooling rate of neat PHBHHx resulted in a mostly amorphous polymer with an X_c of only 0.1% compared to the significantly more crystalline N2 with an X_c of 14% providing more evidence that NBC acts as a nucleating agent when incorporated into PHBHHx.

Isothermal DSC. Isothermal DSC analysis was done to quantify and further understand the crystallisation rate and kinetics of PHBHHx and its composites. Since it was determined *via* non-isothermal crystallisation that PHBHHx crystallizes at approximately 100 °C, the isothermal crystallisation temperature chosen for this study was 100 °C. The isothermal crystallisation peaks for PHBHHx and NBC composites are presented in Fig. 6. The nucleation effect of NBC can be seen in the crystallisation profiles in Fig. 6 where all the composite samples had sharper and narrower exothermal peaks when compared to neat PHBHHx which indicates that they needed lesser time to crystallise.

The calculation for the crystallisation rate is performed *via* the Avrami equation as described by Shazleen *et al.* (2021).[32] First, the isothermal crystallisation peaks from Fig. 6 were integrated within the limits of $t = 0$ and t followed by dividing with the overall crystallisation rate to obtain the relative degree of crystallinity (X_{rel}). The equation used is as described in eqn (1).

$$X_{rel} = \frac{\int_0^t \frac{dH(t)}{dt} dt}{\int_t^\infty \frac{dH(t)}{dt} dt} \quad (1)$$

Using the information obtained from eqn (1), the Avrami eqn (2) can then be used to determine the Avrami exponent, n and

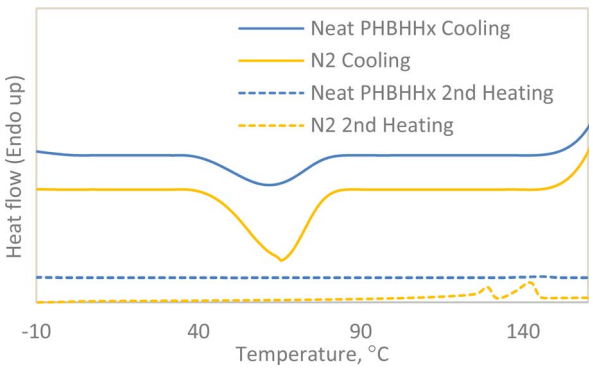

Fig. 5 Non-isothermal cooling (50 °C min^{-1}) followed by second heating (10 °C min^{-1}) curves for neat PHBHHx and N2.

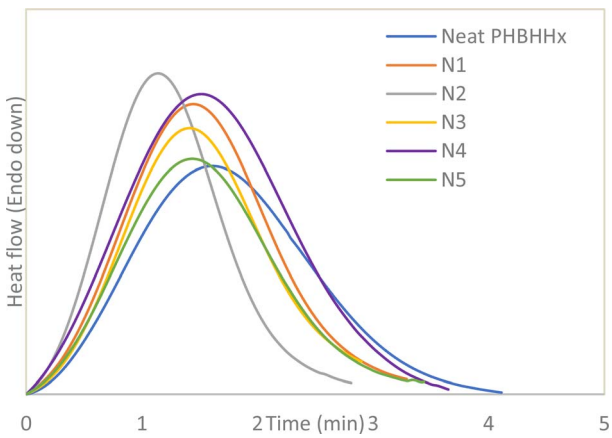

Fig. 6 Isothermal crystallisation profiles for neat PHBHHx and NBC composites.

Table 4 Non-isothermal DSC data for Neat PHBHHx and N2 with cooling rate of 50 °C min^{-1}

Sample	$T_{c\ onset}$ °C	T_c °C	ΔH_c J g^{-1}	T_{m1} °C	T_{m2} °C	ΔH_m J g^{-1}	X_c %
Neat PHBHHx	85	61	20	127	146	0.2	0.1
N2	87	65	38	129	142	20	14

the crystallisation rate constant, k. This is done by modifying eqn (2) into a logarithmic form as shown in eqn (3).

$$X_{rel}(t) = 1 - \exp(-kt^n) \quad (2)$$

$$\log[-\ln(1 - X_{rel}(t))] = n \log t + \log k \quad (3)$$

Eqn (3) allows the plotting of $\log[-\ln(1 - X_{rel}(t))]$ against $\log t$ to form a linear Avrami plot where n is the gradient of the curve, $\log k$ is the y-intercept and t is time. Fig. 7 and 8 presents the plots for X_t *vs.* t and Avrami plots respectively.

With the values of n and k determined, the crystallisation half time, $t_{1/2}$, which is the time taken for the polymer to reach 50% relative crystallinity can then be calculated using eqn (4), of which the reciprocal is the crystallisation rate (eqn (5)):

$$t_{1/2} = \left(\frac{\ln 2}{k}\right)^{1/n} \quad (4)$$

$$\text{Crystallisation rate} = \frac{1}{t_{1/2}} \quad (5)$$

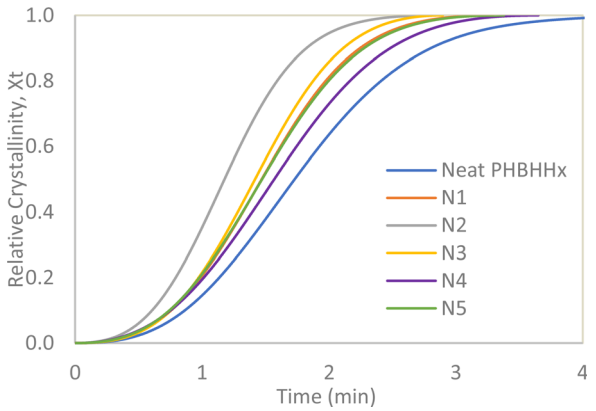

Fig. 7 Relative crystallinity plots for PHBHHx and NBC composites.

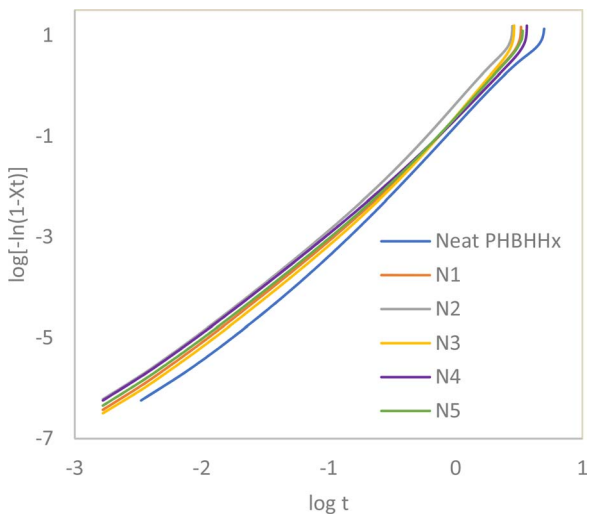

Fig. 8 Avrami plots for neat PHBHHx and NBC composites.

The values from the isothermal crystallisation profiles calculated *via* the series of equations above can be summarized in Table 5. Seeing that the n values of neat PHBHHx and all the composites fall between 2 and 3 and does not differ significantly from each other, it is very likely that the geometry of the crystallites formed mostly conform to two-dimensional shapes in the form of discs.[33] The decrease in the crystallisation half-time occurs from the addition of 1 and 2 wt% NBC resulting in an increase in crystallisation rate of up to 54%. The increase in crystallisation rate suggests that the NBC particles may provide the necessary surface area within the polymer matrix to trigger nucleation of new crystallites. This, together with the increased X_c and T_c from Tables 3 and 4 prove the nucleating properties of NBC. However, an increase in NBC loading above 2 wt% leads to a drop in the crystallisation rate of PHBHHx. As explained in the discussion for non-isothermal DSC analysis, this could be caused by the agglomeration of NBC above a certain composition leading to difficulty of the polymer chains to form crystallite lamellae. Therefore, it can be inferred that the crystallisation rate of PHBHHx in this case depends greatly on the NBC loading.

Tensile properties

The tensile properties of neat PHBHHx and NBC composites are summarised in Table 6. The tensile strength of PHBHHx significantly improved with the incorporation of NBC into its matrix. N2 had the highest tensile strength of 31.6 MPa compared to 27.9 MPa of neat PHBHHx. Previous literature has found mixed results when it comes to the effect of biochar on the tensile strength of polymers. Das *et al.* (2016) found no significant difference in the tensile strength of biochar/PP composites compared to neat PP while Poulose *et al.* (2018) found that biochar reduces the tensile strength of PP.[15,34] Ho *et al.* (2015) however, observed a significant improvement in the tensile strength of PLA with the addition of biochar.[35] It is to be noted that the studies mentioned utilised biochar particles of larger size. In the case of this study, the increase in tensile strength could possibly be attributed to the much larger total surface area of NBC due to their dimensions in the nanometre range which could allow for better dispersion of the particles in the polymer matrix and mechanical interlocking between NBC and the polymer chains. The same case was also observed by Richard *et al.* (2017) where they saw better tensile strength in unsaturated polyester composites containing biochar particles of smaller size (45 nm) compared to those of larger particle dimensions (>45 nm).[22] However, upon NBC loadings higher than 2 wt%, the tensile strengths of the composites start to decrease. This could be due to the occurrence of agglomeration of the NBC particles at higher compositions which effectively increases the size of the filler and worsens their dispersion in the polymer matrix.

Addition of NBC into PHBHHx resulted in increased tensile modulus from 4.8 GPa of neat PHBHHx to up to 5.4 GPa of the composites. Conversely, the ductility of the composites was lower than that of PHBHHx with close to a 50% reduction of elongation at break. This could be due to the combined effect of the rigid properties of biochar and the efficient stress transfer

Table 5 Crystallisation rates and Avrami parameters for PHBHHx and NBC composites

Sample	n	k (min^{-n})	Crystallisation half time, $t_{1/2}$ (min)	Crystallisation rate, $1/t_{1/2}$ (min^{-1})
Neat PHBHHx	2.53	0.158	1.79	0.56
N1	2.58	0.272	1.44	0.70
N2	2.60	0.467	1.16	0.86
N3	2.67	0.283	1.40	0.72
N4	2.42	0.253	1.52	0.66
N5	2.54	0.276	1.44	0.70

Table 6 Tensile properties of neat PHBHHx and NBC composites

Sample	Tensile stress at max load (MPa)	Tensile modulus (GPa)	Elongation at break (%)
Neat PHBHHx	27.9 ± 0.3	4.8 ± 0.1	4.1 ± 0.6
N1	31.4 ± 0.3	5.4 ± 0.2	3.1 ± 0.1
N2	31.6 ± 0.4	5.4 ± 0.1	2.7 ± 0.3
N3	31.0 ± 0.5	5.3 ± 0.3	2.1 ± 0.4
N4	30.8 ± 0.4	5.4 ± 0.1	2.3 ± 0.1
N5	30.6 ± 0.5	5.4 ± 0.1	2.5 ± 0.2

between the PHBHHx and NBC resulting in improved resistance of the composite from deformation and decreased ductility. The results for tensile modulus and elongation at break were also consistent with multiple studies in literature regardless of the type of polymer studied.[13,15,22,35,36] Additionally, the increase in tensile strength and modulus could also be explained by the higher degree of crystallinity of the composites as opposed to neat PHBHHx as explained by the data from DSC analysis. Increase in crystallinity is caused by a more compact and ordered structure of the polymer chains resulting in larger degree of intermolecular interactions between the chains which would then effectively increase the tensile strength and modulus. Consequently, an increase in polymer crystallinity also leads to a decrease in ductility.[36]

Dynamic mechanical properties

DMA analysis was done to investigate both the viscoelastic properties of the NBC composites and their mechanical integrity at elevated temperatures. The storage modulus quantifies the ability of the composites to store energy elastically making it similar to the tensile or Young's modulus in the sense that they both measurements of stiffness. Fig. 9a shows that the addition of up to 3wt% NBC increases the storage modulus of PHBHHx. This means that NBC, depending on the composition, improves the stiffness of PHBHHx which correlates well with the data from tensile testing. The storage modulus of PHBHHx and NBC composites at three different temperatures were extracted from Fig. 9a and compiled in Table 7. The data show that, even at elevated temperatures up to 100 °C, the storage modulus of N1 to N3 were higher than that of neat PHBHHx with the highest being that of N1 with a storage modulus of 260 MPa. This means that the increase in stiffness of the composites were maintained as the temperature increased. The storage modulus values at different temperatures are also potentially higher than that of the commercially available polypropylene.[37] This could prove useful if the composite is intended for applications which require exposure to higher temperatures.

Tan δ measures the dissipation of energy in materials. In other words, it measures the energy damping capabilities in the composites. Tan δ is obtained from the ratio of the loss modulus from Fig. 9b to the storage modulus from Fig. 9a. Fig. 9c shows that there is a decrease in the tan δ peak intensity of PHBHHx with the incorporation of NBC. This implies that the resulting composites exhibit more elastic behaviour as opposed to viscous ones when compared to neat PHBHHx. Thus, the damping or energy dissipation capabilities of the PHBHHx decreases upon the addition of NBC as the composites lean towards energy storage rather than dissipation as the composition of NBC increases. This is explained by the restriction in polymer mobility with the addition of NBC particles leading to a stiffer, less viscous material.

Cell morphology and MTT cell viability of HaCat cells

Alterations in cell morphology are considered a sign of toxicity. As can be seen in Fig. 10, the human epidermal keratinocytes, HaCat cells were viable up to 72 h after exposure to biocomposite samples (PHBHHx and PHBHHx/NBC) with no significant variation in morphology observed across cell areas. The typical flat and polygonal shape of the HaCat cells remained unchanged during the incubation periods of 24 h, 48 h and 72 h. This was an interesting finding because the cells were able to spread out and form a more cobblestone-like appearance at 72 h as a previous study reported similar non-toxic features in the cells.[38] Therefore, it can be concluded that the PHBHHx sample with NBC possess no cytotoxicity effect and can be used as biomaterials.

The *in vitro* cytotoxicity of NBC in PHBHHx was determined for 24 h, 48 h and 72 h using the human epidermal keratinocyte cell line, HaCat for PHBHHx and PHBHHx/NBC, where

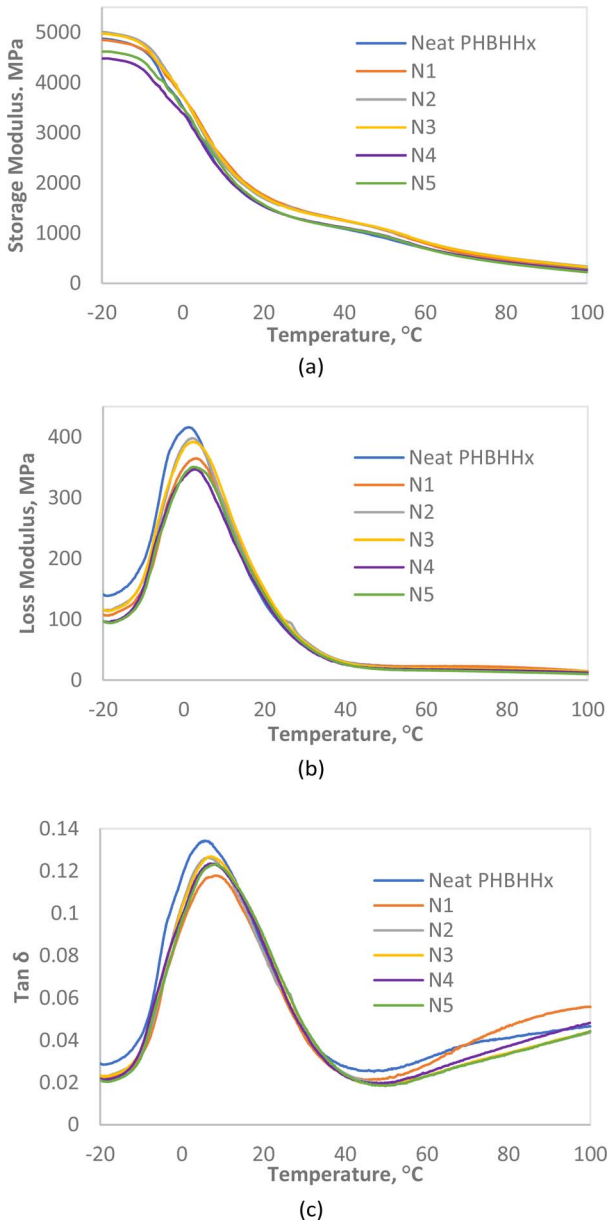

Fig. 9 DMA profiles of Neat PHBHHx and composites: (a) storage modulus, (b) loss modulus, (c) tan δ.

Table 7 Storage modulus of neat PHBHHx and NBC composites at different temperatures

	Storage modulus, E′ (MPa)		
Sample	30 °C	60 °C	100 °C
Neat PHBHHx	1252	697	286
N1	1438	799	260
N2	1422	827	335
N3	1409	827	323
N4	1259	708	251
N5	1248	695	222

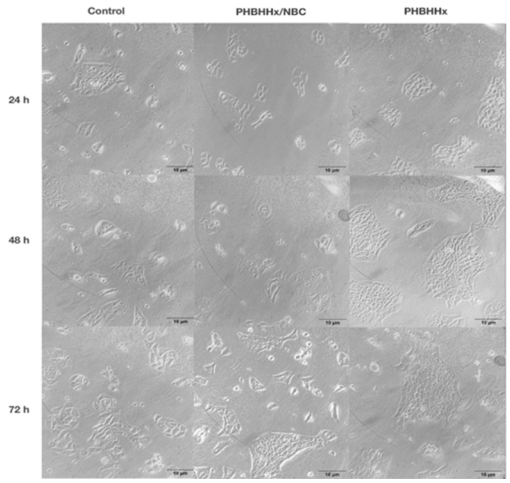

Fig. 10 Morphological profiles of HaCat cells after treatment with PHBHHx, and PHBHHx/NBC. Untreated HaCat cells are used as control. The photos were taken 24 h, 48 h and 72 h post-treatment. The scale bars represent 10 μm.

untreated HaCat cells were used as control. The weight of PHBHHx films was set at 5.0 mg based on a previous study by Rajaratanam *et al.*[27] The MTT assay was used to determine the cytotoxic effect of the biocomposites films. According to the MTT results, all tested substances had no significant cytotoxic effect on HaCat cells, as shown in Fig. 11. All biocomposites samples have cell viability percentages greater than 80% after 24 h, 48 h, and 72 h of exposure, respectively. The control (untreated cells) is deemed to be 100% viable. Cell viability value in the PHBHHx/NBC sample was increased by 24 h and 48 h but slightly decreased by 72 h. On the other hand, the PHBHHx/NBC sample showed increasing value of cell viability at 24 h, 48 h and 72 h. In previous cell viability studies, the PHBHHx films were found to be biocompatible, nontoxic, and even slightly increased the cell viability and cell proliferation rate of the tested cell lines.[27,39,40] For instance, Wang *et al.* (2019)

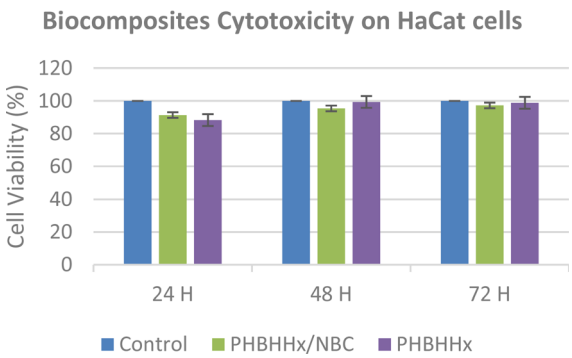

Fig. 11 Cell viability of the biocomposites films towards HaCat cells for 24 h, 48 h and 72 h. The control was represented by the untreated cells. The result shows that the average of triplicate data is represented as mean ± SD. The statistical significance was determined at $p > 0.05$. None of the samples were shown to be significant against the untreated cells.

reported that PHBHHx film has the ability to support cell growth and adhesion of neural stem cells (NSCs) *in vitro* without any side effects.[40]

Conclusions

PHBHHx/NBC bionanocomposites exhibited an increment in the crystallisation rate by 54% compared to neat PHBHHx, indicating the nucleating ability of the NBC. The incorporation of NBC increased the polymer crystallinity and consequently improved the tensile strength and modulus. DMA analysis further proved the ability of the bionanocomposites to maintain their increased stiffness at elevated temperatures when compared to neat PHBHHx. This proves that biochar particles when reduced to nano-size can be functional nucleating agents and reinforcing fillers for biopolymers. Finally, the PHBHHx samples with NBC were found to be non-cytotoxic for the growth of human epidermal keratinocytes, HaCat.

Author contributions

All authors contributed to the study conception and design. Material preparation, data collection and analysis were performed by L. Y. F. N, M. S., T. K., T. T., T. A. T. Y., and N. M. A. N. A. R. The first draft of the manuscript was written by L. Y. F. N. Funding acquisition was handled by H. A. The study was supervised by H. A., O. Y. and M. A. H. All authors commented on previous versions of the manuscript. All authors read and approved the final manuscript.

Conflicts of interest

There are no conflicts of interest to declare.

Acknowledgements

The authors would like to express gratitude to the Malaysian Ministry of Higher Education for the provision of Fundamental Research Grant Scheme (vot no: 5540321 and project code: FRGS/1/2019/TK05/UPM/02/1).

References

1 A. Chamas, H. Moon, J. Zheng, Y. Qiu, T. Tabassum, J. H. Jang, M. Abu-Omar, S. L. Scott and S. Suh, *ACS Sustain. Chem. Eng.*, 2020, **8**, 3494–3511.
2 M. Suzuki, Y. Tachibana and K. ichi Kasuya, *Polym. J.*, 2021, **53**, 47–66.
3 H. Sashiwa, R. Fukuda, T. Okura, S. Sato and A. Nakayama, *Mar. Drugs*, 2018, **16**, 1–11.
4 K. W. Meereboer, M. Misra and A. K. Mohanty, *Green Chem.*, 2020, **22**, 5519–5558.
5 Y. Doi, S. Kitamura and H. Abe, *Macromolecules*, 1995, **28**, 4822–4828.
6 H. M. Chang, Z. H. Wang, H. N. Luo, M. Xu, X. Y. Ren, G. X. Zheng, B. J. Wu, X. H. Zhang, X. Y. Lu, F. Chen, X. H. Jing and L. Wang, *Braz. J. Med. Biol. Res.*, 2014, **47**, 533–539.
7 Q. Zhang, Q. Liu, J. E. Mark and I. Noda, *Appl. Clay Sci.*, 2009, **46**, 51–56.
8 J. Vandewijngaarden, R. Wauters, M. Murariu, P. Dubois, R. Carleer, J. Yperman, J. D'Haen, B. Ruttens, S. Schreurs, N. Lepot, R. Peeters and M. Buntinx, *J. Polym. Environ.*, 2016, **24**, 104–118.
9 A. Niemczyk, K. Dziubek, B. Sacher-Majewska, K. Czaja, J. Czech-Polak, R. Oliwa, J. Lenza and M. Szołyga, *Polymers*, 2018, **10**, 1019.
10 I. Dubdub and M. Al-Yaari, *Polymers*, 2020, **12**, 891.
11 International Flight Services Association (IFSA) and Association of European Airlines (AEA), *World Food Safety Guidelines for Airline Catering*, 2010.
12 J. Vandewijngaarden, M. Murariu, P. Dubois, R. Carleer, J. Yperman, J. D'Haen, R. Peeters and M. Buntinx, *J. Appl. Polym. Sci.*, 2016, **133**, 1–10.
13 O. Das, N. K. Kim, A. K. Sarmah and D. Bhattacharyya, *J. Clean. Prod.*, 2017, **144**, 79–89.
14 M. Naghdi, M. Taheran, R. Pulicharla, T. Rouissi, S. K. Brar, M. Verma and R. Y. Surampalli, *Arab. J. Chem.*, 2019, **12**, 5292–5301.
15 A. M. Poulose, A. Y. Elnour, A. Anis, H. Shaikh, S. M. Al-Zahrani, J. George, M. I. Al-Wabel, A. R. Usman, Y. S. Ok, D. C. W. Tsang and A. K. Sarmah, *Sci. Total Environ.*, 2018, **619–620**, 311–318.
16 A. A. Alghyamah, A. Yagoub Elnour, H. Shaikh, S. Haider, A. Manjaly Poulose, S. M. Al-Zahrani, W. A. Almasry and S. Young Park, *J. King Saud Univ., Sci.*, 2021, **33**, 101409.
17 N. Nan, D. DeVallance, X. Xie and J. Wang, *J. Compos. Mater.*, 2015, **50**, 1161–1168.
18 Q. Zhang, H. Cai, X. Ren, L. Kong, J. Liu and X. Jiang, *Polymers*, 2017, **9**, 628.
19 M. Idrees, S. Jeelani and V. Rangari, *ACS Sustain. Chem. Eng.*, 2018, **6**, 13940–13948.
20 M. A. Ashraf, W. Peng, Y. Zare and K. Y. Rhee, *Nanoscale Res. Lett.*, 2018, **13**, 214.
21 H. M. Hassanabadi and D. Rodrigue, *Macromol. Mater. Eng.*, 2014, **299**, 1220–1231.
22 S. Richard, J. Selwin Rajadurai and V. Manikandan, *J. Tribol.*, 2017, **139**, 012202.
23 Q. Dou and J. Xue, *J. Macromol. Sci., Part B*, 2015, **54**, 947–961.
24 L. Y. F. Ng, H. Ariffin, T. A. T. Yasim-Anuar, M. A. A. Farid and M. A. Hassan, *Nanomaterials*, 2022, **12**, 3251.
25 L. Lou, L. Luo, L. Wang, G. Cheng, X. Xu, J. Hou, B. Xun, B. Hu and Y. Chen, *J. Colloid Interface Sci.*, 2011, **361**, 226–231.
26 Y. Hussin, M. N. Mubin Aziz, N. F. Che Rahim, S. K. Yeap, N. E. Mohamad, M. J. Masarudin, N. Nordin, N. M. A. N. Abd Rahman, C. Y. Yong and M. N. Akhtar, *J. Mol. Sci.*, 2018, **19**, 1151.
27 D. D. Rajaratanam, H. Ariffin, M. A. Hassan, N. M. A. N. Abd Rahman and H. Nishida, *PLoS One*, 2018, **13**, 1–14.
28 H. Ariffin, H. Nishida, M. A. Hassan and Y. Shirai, *Biotechnol. J.*, 2010, **5**, 484–492.
29 O. Das, D. Bhattacharyya, D. Hui and K. T. Lau, *Composites, Part B*, 2016, **106**, 120–128.

30 Y. Hu, J. Zhang, H. Sato, I. Noda and Y. Ozaki, *Polymer*, 2007, **48**, 4777–4785.
31 S. S. Shazleen, T. A. T. Yasim-Anuar, N. A. Ibrahim, M. A. Hassan and H. Ariffin, *Polymers*, 2021, **13**, 1–19.
32 S. S. Shazleen, L. Y. F. Ng, N. A. Ibrahim, M. A. Hassan and H. Ariffin, *Polymers*, 2021, **13**, 3226.
33 V. Hinrichs, G. Kalinka and G. Hinrichsen, *J. Macromol. Sci., Part B*, 1996, **35**, 295–302.
34 O. Das, A. K. Sarmah and D. Bhattacharyya, *Waste Manag.*, 2016, **49**, 560–570.
35 M. P. Ho, K. T. Lau, H. Wang and D. Hui, *Composites, Part B*, 2015, **81**, 14–25.
36 S. J. A. Hocker, W. T. Kim, H. C. Schniepp and D. E. Kranbuehl, *Polymer*, 2018, **158**, 72–76.
37 J. L. Rivera-Armenta, B. A. Salazar-Cruz, A. C. Espindola-Flores, D. S. Villarreal-Lucio, C. M. De León-Almazán and J. Estrada-Martinez, *Appl. Sci.*, 2022, **12**, 8336.
38 C. Devandran, J. Carthew, J. E. Frith and A. Neild, *Advanced Science*, 2019, **6**, 1902326.
39 F. Ghaemi, L. C. Abdullah, N. M. A. N. Abd Rahman, S. U. F. Syed Najmuddin, M. M. Abdi and H. Ariffin, *Res. Chem. Intermed.*, 2017, **43**, 4981–4991.
40 L. Wang, Z. Yang, F. Fan, S. Sun, Z. Wu, H. Lu and X. Lu, *Biomacromolecules*, 2019, **20**, 3294–3302.